

**A Novel Automatic Real-time Motion Tracking Method for Magnetic Resonance Imaging-guided Radiotherapy: Leveraging the Enhanced Tracking-Learning-Detection Framework with Automatic Segmentation**

Shengqi Chen<sup>1</sup>;

Zilin Wang<sup>1</sup>;

Jianrong Dai<sup>2</sup>;

Shirui Qin<sup>2</sup>;

Ying Cao<sup>2</sup>;

Ruiao Zhao<sup>2</sup>;

Jiayun Chen<sup>2\*</sup>; (Corresponding author, Email: grace\_chenjy@163.com)

Guohua Wu<sup>1\*</sup>; (Corresponding author, Email: wuguohua@bupt.edu.cn )

Yuan Tang<sup>2\*</sup>; (Corresponding author, Email: tangyuan82@126.com )

\* These authors contributed equally to this work. Jiayun Chen, Guohua Wu and Yuan Tang contributed equally as corresponding authors

<sup>1</sup> School of Electronic Engineering, Beijing University of Posts and Telecommunications, Beijing, China

<sup>2</sup> Department of Radiation Oncology, National Cancer Center/National Clinical Research Center for Cancer/Cancer Hospital, Chinese Academy of Medical Sciences and Peking Union Medical College, Beijing, China

**【Abstract】**

**Objective:** Ensuring the precision in motion tracking for MRI-guided Radiotherapy (MRIgRT) is crucial for the delivery of effective treatments. This study refined the motion tracking accuracy in MRIgRT through the innovation of an automatic real-time tracking method,

leveraging an enhanced Tracking-Learning-Detection (ETLD) framework coupled with automatic segmentation.

**Methods:** We developed a novel MRIgRT motion tracking method by integrating two primary methods: the ETLD framework and an improved Chan-Vese model (ICV), named ETLD+ICV. The TLD framework was upgraded to suit real-time cine MRI, including advanced image preprocessing, no-reference image quality assessment, an enhanced median-flow tracker, and a refined detector with dynamic search region adjustments. Additionally, ICV was combined for precise coverage of the target volume, which refined the segmented region frame by frame using tracking results, with key parameters optimized. Tested on 3.5D MRI scans from 10 patients with liver metastases, our method ensures precise tracking and accurate segmentation vital for MRIgRT.

**Results:** An evaluation of 106,000 frames across 77 treatment fractions revealed sub-millimeter tracking errors of less than 0.8mm, with over 99% precision and 98% recall for all subjects, underscoring the robustness and efficacy of the ETLD. Moreover, the ETLD+ICV yielded a dice global score of more than 82% for all subjects, demonstrating the proposed method's extensibility and precise target volume coverage.

**Conclusions:** This study successfully developed an automatic real-time motion tracking method for MRIgRT that markedly surpasses current methods. The novel method not only delivers exceptional precision in tracking and segmentation but also demonstrates enhanced adaptability to clinical demands, positioning it as an indispensable asset in the quest to augment the efficacy of radiotherapy treatments.

**【 Key words 】** Real-time Tracking Method, Enhanced Tracking-Learning-Detection

## 1. Introduction

Radiotherapy stands as a pivotal treatment modality within clinical oncology, offering the benefits of efficiently targeting tumors while safeguarding adjacent healthy tissues. It is noteworthy that approximately 70% of cancer patients receive radiotherapy at some point in their treatment journey[1, 2]. The fundamental objective of radiotherapy is to deliver concentrated radiation doses to the tumor volume, sparing the surrounding healthy tissues as much as possible [3, 4]. However, intra-fraction motion, driven by physiological processes such as respiration and gastrointestinal activity, can result in tumor position shifts with average amplitudes ranging from 2-14mm[5]. These displacements have the potential to compromise the optimal delivery of radiation doses to the target volume and may inadvertently increase the dose to healthy tissues, thus threatening the efficacy of the treatment [3, 6]. A wealth of evidence from several studies underscores this point. In the context of abdominal regions, one study demonstrated that even minor intra-fraction motion (mean error < 8mm) can lead to a significant reduction of up to 24% in the radiation dose to the liver [7]. Another study reported that in scenarios lacking motion adaptation, for a planning target volume (PTV) with a cranio-caudal margin of 7 mm, liver tumors exhibited an average geometric error of less than 10 mm, yet the radiation dose they received was diminished by more than 29%[8]. Similarly, research focusing on the pancreas revealed that mean motion amplitudes of 9.6 mm in the cranio-caudal direction and 6.9 mm in the anterior-posterior direction could culminate in a 28% reduction of

the prescribed dose to the clinical target volume (CTV)[9]. The accurate compensation for such shifts is imperative to ensure that the tumor is delivered the prescribed radiation dose while mitigating the effects on healthy tissues. Consequently, the meticulous management of intra-fraction motion has become a critical area of focus for enhancing patient outcomes[6, 10]. Precision radiotherapy, capable of accounting for these subtle but significant motions, has indeed established a new benchmark for treating advanced cancers[11].

Image-guided radiotherapy (IGRT) represents a cornerstone strategy for achieving precision radiotherapy[2, 12]. While cone-beam CT (CBCT) is prevalent for online tumor positioning verification in IGRT, it has limitations, including extended scanning times, increased imaging doses, and limited tissue contrast[13]. Some studies have explored the use of tumor surrogates, such as the diaphragm and chest wall, for tracking purposes[14, 15]. However, the correlation between tumor motion and surrogates can vary significantly among individuals[16]. Other approaches have involved the invasive implantation of gold fiducials within tumors for tracking[17, 18], which introduces discomfort and potential uncertainties[4, 19].

Magnetic resonance imaging-guided radiotherapy (MRIgRT) distinguishes itself from traditional X-ray-guided radiotherapy by offering superior soft tissue contrast and the capability for real-time imaging during treatment. These attributes facilitate more accurate tumor targeting and reduce radiation toxicity to healthy tissues[12, 20]. Despite its early clinical adoption, MRIgRT has demonstrated substantial benefits for cancer patients[21, 22]. The development of accelerated imaging methods has made MRIgRT increasingly viable for online treatment plan adaptation[2, 23, 24]. The deployment of MRI-Linacs in clinical settings provides comprehensive information throughout the treatment process, supporting both manual and

automated decision-making [20]. It is envisioned that MRIgRT will play a transformative role in IGRT.

In the context of MRIgRT, physicians can adjust the planning target volume (PTV) dynamically during treatment[20]. Nonetheless, current MRIgRT systems often rely on manual contouring to determine the target's projection in various views, which is inefficient and prone to inconsistencies[25]. Additionally, imaging artifacts and deformations can impair the interpretation of radiographs by clinicians[26]. To address these challenges, several studies have investigated automated, markerless motion management during radiotherapy based on MRI[27-36], offering the advantage of being non-invasive and beneficial to patients. Among these, machine learning-based methods have been employed for motion estimation of the target[27-30, 32, 34], but further refinement is necessary to attain sub-millimeter accuracy. Some methods are not end-to-end, necessitating additional steps[27, 28]. Deep learning (DL) is another possible way, reliant on pre-trained models[33, 35, 36]. Its application to newly developed MRI imaging sequences is challenging due to the requirement for extensive datasets for training. The scarcity of available data for these new sequences[25] limits the feasibility of DL, as it traditionally relies on large volumes of data to create robust, pre-trained models. Discrepancies between training and test sets can diminish accuracy, resulting in unpredictable performance when models are applied to new datasets. Furthermore, inconsistencies in manually labeled ground truth can impose constraints on the deep learning training process[4]. This limitation underscores the need for alternative or innovative methods that can adapt to the limited data scenarios often encountered with novel imaging technologies. Therefore, we introduce the Tracking-Learning-Detection (TLD) framework[37], a high-performance method

for object tracking that has been successfully used for tasks such as moving vehicle tracking[38] and pedestrian tracking[39]. This framework has also preliminarily demonstrated its suitability for motion management in MRIgRT, capable of adapting to the target volume's disappearance and deformation[34]. However, the study also reported notable tracking failures with the TLD under 0.35T MRI, while high precision in tracking has consistently been a critical requirement in clinical radiotherapy.

In this study, we introduce an innovative and comprehensive tracking method designed to tackle the challenge of real-time target motion management during MRIgRT. Our method is anchored in an enhanced Tracking-Learning-Detection algorithm, specifically adapted for the high spatial and temporal resolution imaging sequences characteristic of MRI, complemented by an advanced automatic segmentation method. By integrating image pre-processing with a no-reference image quality assessment (NRIQA), our method circumvents the need for pre-training, thereby attaining tracking accuracy at the sub-millimeter. This advancement not only ensures precise tracking of target volumes but also maintains the high-accuracy standards required for real-time applications. The efficacy of our proposed method is substantiated through rigorous validation of a dataset of MRI images, demonstrating its potential to significantly enhance the precision and efficiency of MRIgRT procedures.

## 2. Materials and Methods

### 2.1. High Spatial and Temporal Resolution MRI Method with BEV/BPV Fusion Information

A recent research team has developed an innovative high spatial and temporal resolution MRI method that seamlessly integrates Beam Eye View (BEV) and Beam Path View (BPV) fusion information, designated as 3.5D MRI[2]. This advanced method optimizes the alignment of the MRI centroid with the radiation beam's center, generating 3 orthogonal imaging planes that are inherently tailored to the tumor's centroid and the radiation field's orientation. Specifically, it produces two BPV planes aligned with the radiation rays and one BEV plane perpendicular to these rays, providing precise, real-time localization of the target volume and organs at risk (OARs) without necessitating post-processing adjustments.

## **2.2. Data Acquisition**

Patients with colorectal cancer liver metastasis treated with the MR-Linac Unity (Elekta AB, Stockholm, Sweden) were selected excluding those with contraindications to radiotherapy. Patient positioning was performed using a CT simulation localization system for 4D-CT scanning (Siemens Healthcare, Erlangen, Germany), with the patient in a supine position, arms raised and supported on a headrest bracket. Target volume delineation was performed based on the scanned images, and the treatment plan was devised using the Monaco Version 5.4 system (Elekta AB, Stockholm, Sweden) for intensity-modulated radiotherapy (IMRT), employing 6-9 beams. During treatment, the patients followed a standard protocol using an abdominal compression belt to limit abdominal movement, and 2D cine MR imaging was utilized for continuous tumor position monitoring to ensure dose delivery accuracy. After each treatment, the abdominal compression belt was reapplied to restrict abdominal movement, and 3.5D MRI data (group RAM) was acquired. Subsequently, patients were scanned in a free-breathing state

to obtain 3.5D MRI data (group FB).

The study included a total of 10 patients, with 3.5D MRI images collected from multiple treatment fractions, captured frame by frame across one BEV plane (transverse) and two BPV planes (coronal, and sagittal) intersecting at the treatment isocenter with 50 frames per plane at a frequency of 4.347 Hz. By selecting 2D cine MRI images from the coronal and sagittal planes, we compiled a high-quality MRI tracking dataset comprising 112,800 frames from 77 treatment fractions, totaling 2,256 data sets. The resolution of each frame ranges from 320 × 320 to 560 × 560 pixels, and the spacing ranges from 0.571 × 0.571 to 0.938 × 0.938 mm. Variability in angles between the longitudinal cine-MRI imaging and coronal planes, as well as intervals, is noted among different patients.

### **2.3. Data Preprocessing**

The patient data, acquired through 3.5D MRI protocol, exhibited relatively high imaging quality compared to vendor-provided cine-MRI[2]. However, the spatial resolution and signal-to-noise ratio (SNR) did not match the levels seen in natural images. The image sequences often presented with inconsistent brightness, low contrast, and significant noise. To enhance the images for better alignment with the TLD tracking assumptions[37], a series of preprocessing steps were applied.

Specifically, all images underwent grayscale normalization to correct for brightness inconsistencies. To further refine the image quality, gamma correction was implemented to enhance contrast, and a Gaussian filter was applied to smooth out noise. Throughout the experimental phase, a comprehensive trial of 23 different preprocessing methods and their

potential combinations was conducted. The final preprocessing scheme was selected based on its performance in the no-reference image quality assessment (NRIQA) method (section 2.4), ensuring the effectiveness of the preprocessing steps as described in this section.

#### **2.4. No Reference Image Quality Assessment (NRIQA)**

The NRIQA provides a crucial solution for medical imaging environments lacking high-quality reference images, as it operates without the need for comparative training data[40]. Utilizing median absolute deviation (MAD) weighting, NRIQA dynamically scores image quality, aligning with clinical demands and pioneering a new direction in medical image processing where no-reference assessments were previously unexplored.

Our evaluation of preprocessing schemes through NRIQA identified the optimal strategy by selecting the one with the highest average quality score, as described in Section 2.3. To maintain data effectiveness, an admission mechanism filters MRI data below a threshold  $T$ , set at the 5<sup>th</sup> percentile of scores, which was empirically chosen and validated by a radiation oncologist to ensure sufficient data quality and reduce unnecessary processing.

#### **2.5. Enhanced Tracking-Learning-Detection (ETLD)**

The original Tracking-Learning-Detection (OTLD) framework, a machine learning algorithm adept at long-term tracking of a single target within video streams[37], has been meticulously refined for our study. This improved version termed the Enhanced Tracking-Learning-Detection (ETLD) method, integrates several key enhancements to fortify its adaptability and precision for real-time MRI-guided tracking scenarios.

The ETLD keeps the main modules of the OTLD, which comprises 3 principal components: an

inter-frame motion estimator, a detector for potential target locations exploration, and a learning module that dynamically updates the detector's capabilities. As shown in Figure 1, the ETLD contains 4 stages, where pre-processed cine-MRIs are used as inputs to the algorithm, and are processed by the tracking, detection, and learning modules before being integrated by the integrator as a unique location prediction. These components have been subject to a series of optimizations, and the main improvements are highlighted in red rounded rectangles detailed as follows:

- 1) Image Preprocessing and Quality Enhancement: To ensure the ETLD's tracker operates optimally, images undergo preprocessing to refine their quality, making them more conducive to accurate tracking, as illustrated in sections 2.3 and 2.4.
- 2) Search Process Optimization: Considering that typical targets to be tracked are usually small and their sizes usually do not change significantly. Thus, we reduced the minimum window size for window scanning and the normalized size of the image patch to accommodate small targets. Additionally, we decreased the scaling factor of the sliding windows from 1.2 to 1.1 to better search for potential target locations.
- 3) Median-Flow Tracker Enhancement: Our refinements to the median-flow tracker are specifically aimed at capturing the intricate motion dynamics of small targets with greater accuracy. We have streamlined the pyramidal Lucas-Kanade optical-flow tracker by reducing the number of pyramid levels to 3, which is more adept at identifying the subtle movements of these targets. To further enhance the precision of the tracker, we have expanded the neighborhood size of the Lucas-Kanade (LK) algorithm to 31 pixels and increased the number of iterations the algorithm performs. These adjustments allow for a more nuanced analysis of

the target's trajectory, ensuring that our tracking results are as exact as possible.

4) Dynamic Search Region Adjustment: Drawing from a previous study[2] that reported the maximum 95th percentile displacement of liver tumors to be approximately 10 mm, we have strategically confined the detector's search region. This refinement shifts from a comprehensive global search to a more focused, dynamically updated regional search. We have delineated the search region to a compact  $30 \times 30$ -pixel area, anchored at the centroid of the target's location derived from the preceding 3 frames. This targeted method significantly minimizes the likelihood of encountering false positives, enhancing the overall accuracy and efficiency of the tracking process.

## **2.6. Automatic Segmentation Process**

Beyond the mere bounding box output typical of position prediction, the incorporation of semantic segmentation in our process ensures that the radiotherapy beam precisely covers the region of interest (ROI). To achieve this, we have coupled a proven segmentation method with our ETLD method, utilizing the Chan-Vese model[41]. The Chan-Vese model is adept at contouring the target volume through an iterative process that minimizes an energy function, enhanced with regularization terms, a method well-established in the realm of medical image segmentation[42].

Typically, the Chan-Vese model takes a global image sequence and a fixed mask as input to achieve contour segmentation. For our specific implementation, in addition to the global image, the initial frame's target bounding box serves as a foundational input to the segmentation model. Concurrently, the ETLD's calculated predictions of the target's central coordinates in each

subsequent frame provide a dynamic, frame-by-frame refinement. These inputs thus are harmoniously combined within the segmentation model to achieve an automatic segmentation process that is both accurate and responsive to the subtleties of the target's shape and position throughout the treatment sequence. Additionally, we refined the model parameters, including the number of iterations, to ensure segmentation accuracy while meeting real-time performance requirements. For ease of reference, we have designated our integrated approach, which combines the enhanced Tracking-Learning-Detection (TLD) framework with the improved Chan-Vese model, named as the ETLD+ICV method. This ETLD+ICV method not only promises a higher degree of precision in radiotherapy beam targeting but also streamlines the segmentation process, making it more efficient and reliable for clinical applications.

## 2.7. Evaluation Procedure

Our proposed tracking method, crafted in C++ and MATLAB, optimizes location prediction based on online learning, thereby eliminating the need for pre-training. This streamlined method was executed on a high-performance PC, equipped with a 13th Gen Intel(R) Core(TM) i9-13980HX processor and a substantial 32GB of RAM. Notably, our method's efficiency negates the requirement for GPU acceleration, making it highly accessible. The experiments were conducted within a Windows 11 environment, leveraging the robust capabilities of Visual Studio 2019 in conjunction with the OpenCV 3.3.1 library.

Given the subtlety of tumor delineation in 3.5D MRI, we opted to track blood vessels as a proxy for tumor motion. This strategy is supported by a robust body of evidence that demonstrates a strong positive correlation between liver tumors and blood vessel motion[43, 44], rendering

blood vessels a reliable surrogate for our study. The proposed method's efficacy was meticulously evaluated using an extensive dataset, encompassing data from 10 patients and comprising 112,800 frames.

To ensure the highest standard of evaluation, the ground truth was established through manually curated binary masks of tumor regions by radiation oncologists, reflecting the irregular shapes of liver tumors. This meticulous process was dually verified, a testament to our commitment to accuracy. The entire data verification process, which spanned 9 months, was necessitated by the vast dataset, during which poor-quality images were meticulously excluded. Following the stringent application of our admission criteria, the dataset was refined to 2,120 sets of high-quality data, amassing 106,000 frames. This rigorous verification procedure underscores our method's robustness.

## **2.8. Evaluation Metrics**

The prowess of our proposed method is stringently appraised through a battery of precise metrics, delineated as follows:

### **2.8.1. Tracking Performance Evaluation**

Ensuring that the radiation beam adheres to the tumor center's trajectory with meticulous precision is of paramount importance in clinical settings. To mirror this clinical priority, we simulated the radiotherapy beam's real-time trajectory using our tracking algorithm's output.

The mean absolute error (MAE) has been embraced as the cornerstone metric for this assessment, as articulated in Equation (1):

$$MAE = \frac{1}{N} \sum_{i=1}^N |\vec{P}_i - \vec{G}_i| \quad (1)$$

In this formulation,  $\vec{P}_i$  and  $\vec{G}_i$  denote the predicted and actual displacement vectors at frame  $i$ , respectively, with  $|\cdot|$  signifying the absolute value.  $N$  represents the number of frames. This metric serves as a quantifiable reflection of the tracking algorithm's fidelity to the tumor's motion.

To further substantiate the tracking efficacy, the correlation coefficient (CC) was deployed, where a superior CC value is indicative of exemplary tracking, as corroborated by previous research[45]. We have also determined the precision and recall rates for the algorithm across the patients' dataset, offering a granular evaluation of its clinical applicability.

### 2.8.2. Segmentation Performance Evaluation

For the segmentation facet, the Dice coefficient, a standard in the field, is employed as depicted in Equation (2):

$$Dice = \frac{2|mask_i^{prediction} \cap mask_i^{groundtruth}|}{|mask_i^{prediction}| + |mask_i^{groundtruth}|} \quad (2)$$

Here,  $mask_i^{prediction}$  symbolizes the algorithm's predicted mask output, while  $mask_i^{groundtruth}$  represents the ground truth. The intersection of these masks is denoted by  $\cap$ , and  $|\cdot|$  quantifies the pixel count. In our experiments, the dice global metric, highlighted in the Liver Tumor Segmentation Challenge (LiTS) competition[46], was utilized to evaluate the segmentation efficacy. This metric is particularly adept at capturing the algorithm's overall performance, especially considering the variance in target sizes and the sensitivity of the Dice coefficient to contour estimation[47].

### 2.8.3. Computational Efficiency Evaluation

The method's real-time capabilities are encapsulated by the frames per second (FPS) metric.

We have meticulously calculated the tracking and segmentation FPS for each patient in our test cohort and subsequently derived an average to present a holistic view of the method's computational efficiency. This metric is pivotal in ensuring that our method meets the stringent time constraints of real-time applications in clinical radiotherapy.

## 3. Results

### 3.1. Accuracy of motion estimation

Figure 2 illustrates the exemplary tracking outcomes of the ETLD on the whole treatment course within the RAM group of one selected patient at 140 gantry angle. The displacement changes are depicted in the graph, with the red line signifying the actual trajectory and the blue line indicating the algorithm's predictions. The juxtaposed images showcase representative frames, highlighting the minimal divergence between predictions and ground truth, thus evidencing a robust correlation.

Figure 3 and Table 1 present a comparative analysis of the tracking performance between our proposed ETLD and the OTLD method across the entire dataset. The MAE box plot in Figure 3(a) demonstrates that the ETLD maintains tracking errors predominantly within a 1 mm threshold, with occasional outliers. The ETLD exhibits tracking over 99% precision and 98% recall, as illustrated in Figure 3(b) and (c). Comparatively, the OTLD falls short in precision and recall. It is noteworthy that the MAE calculation does not account for tracking failures,

which may explain the similarity in the MAE box plots for both ETLD and OTLD.

Table 1 delineates the ETLD average MAE at less than 0.8 mm for all patients, with CC surpassing 94%. Except for the sixth patient, the ETLD outperforms the OTLD across all metrics, including MAE, CC, precision, and recall. This disparity is attributed to the OTLD's higher rate of tracking failures, which are not factored into the MAE calculation. Overall, the ETLD demonstrates precision and recall rates above 99%, with an average tracking error below 0.65 mm and a CC above 96%. In stark contrast, the OTLD's precision rate is below 96%, and its recall rate is less than 77%, with a CC below 95%, suggesting that a significant proportion of targets were not successfully tracked. It is observed that the OTLD's average MAE remains within 1 mm, a result of its low recall rate.

We conducted an in-depth assessment of the algorithm's precision by employing a one-pass evaluation across varying location error thresholds, a method commonly referenced as the precision plot in the domain of object tracking[48]. In tandem, a recall plot was crafted, as depicted in Figure 4. This analysis reveals that the ETLD reliably identifies a broader spectrum of targets at diverse error thresholds, outperforming the OTLD by successfully tracking targets that elude it. A location error threshold of 20 was meticulously chosen to ascertain the definitive precision and recall rates, as exemplified in Figure 3 and Table 1.

### 3.2. Accuracy of Target Segmentation

Considering that the segmentation process is implemented based on tracking results, and ETLD has demonstrated significantly better tracking performance compared to OTLD, we did not implement the combination of OTLD with the ICV method. Figure 5 elucidates the

segmentation performance achieved by the synergistic application of the ETLD+ICV method.

In Figure 5(a), the segmentation results for a sample patient across various treatment fractions are exhibited, with the ground truth demarcated by red outlines and the algorithmic predictions indicated by blue outlines. A stark congruence is observable between the calculated masks and the ground truth, underscoring the algorithm's fidelity. Figure 5(b) encapsulates the statistical aggregation of the segmentation outcomes for each enrolled patient. It is noteworthy that the dice global values surpass 82% across the board. Moreover, the mean dice global value, standing at 87.7%, attests to the robust performance of the proposed automatic segmentation protocol, affirming its efficacy in delineating target volume with high precision.

### 3.3. Computational Efficiency of Tracking and Segmentation

Our experiments were meticulously conducted in batches, aligned with the hardware specifications described in Section 2.7. Without GPU acceleration, our method still performed well. Post-exclusion of the initialization phase, the mean processing frame rate was  $22.304 \pm 7.733$  FPS for tracking and  $25.180 \pm 16.116$  FPS for segmentation.

It is essential to acknowledge that the processing time, as proposed by our method, exhibits variability across the patient cohort. Nevertheless, the overarching average processing time per frame was calculated to be under 50 milliseconds for tracking and below 40 milliseconds for segmentation. These figures collectively demonstrate that our method is highly efficient, with a total processing time that does not exceed 100 milliseconds per frame. This level of performance underscores the method's suitability for real-time radiotherapy applications, where swift and seamless processing is paramount.

#### 4. Discussion

This study critically examines the constraints of prevailing methods in the arena of precision radiotherapy, comparing them with the merits of MRI-guided Radiotherapy (MRIgRT). MRIgRT stands out as a superior alternative, offering heightened soft tissue contrast and eliminating the necessity for marker implantation[20]. To bolster the precision and reliability of target volume motion estimation, we introduce an innovative, comprehensive tracking method. This method, underpinned by a TLD framework, integrates tracking with detection, thereby enhancing adaptability to target disappearances and deformations[37]. Additionally, a segmentation module based on the Chan-Vese model is coupled to further refine the target volume contours.

The OTLD algorithm, recognized for its high-performance tracking solution, has been successfully applied to MRI target tracking[34]. However, it faced challenges with tracking failures and inaccuracies due to differences in signal-to-noise ratios between natural images and MRI images, which is a common issue for motion management in MRIgRT. Given the stringent precision requirements in radiotherapy, we enhanced the OTLD algorithm, resulting in the ETLD. Our improvements included image preprocessing, search process optimization, dynamic search region adjustment, and an enhanced median-flow tracker. To reduce biases associated with image quality, we conducted experiments utilizing MRI data from higher magnetic field strengths (1.5T) and implemented an admission mechanism to filter out low-quality MRI data. Furthermore, since the OTLD algorithm solely provides location predictions, we coupled the

established Chan-Vese segmentation method with the ETLD to ensure precise coverage of the ROI. To the best of our knowledge, this improvement is innovative, as most existing studies focus solely on either tracking or segmentation, whereas the proposed method considers the combination of both. We believe this approach overcomes the limitations of relying solely on a single objective, providing a more comprehensive solution and new insights for motion tracking for radiotherapy. Our proposed method's tracking capabilities were validated using a 3.5D MRI dataset, which encompasses 106,000 frames across 77 fractions after exclusion. The results are promising, with an average MAE of less than 0.8 mm, a CC exceeding 94.3%, and both precision and recall rates surpassing 98% for all test patients. These figures stand in stark contrast to the OTLD method, demonstrating a higher incidence of tracking errors, with overall recall and precision rates falling short of the proposed method. Compared to similar prior studies, our method excels in tracking performance on a substantially larger dataset, with a tracking latency of less than 50 ms, comfortably below the "real-time" threshold of 500 ms as defined by the AAPM Task Group 264[49]. Meanwhile, the ETLD+ICV method achieved excellent segmentation performance, with a dice global exceeding 82% on all patient data, an average dice global of 87.7%, and a processing time of less than 40 ms. This performance is comparable to the results obtained by the U-net model in MRI segmentation[33]. Notably, this performance was achieved without the use of powerful GPUs, indicating potential for cost-effective deployment.

The evolution of real-time MRI-guided radiotherapy is still in its nascent stages. Early studies, such as those by Yun J et al., utilized pulse-coupled neural networks (PCNN) for lung tumor tracking, achieving tracking errors within 3.5 mm, albeit with patient-specific parameters

requiring extensive pre-training[27, 28]. Another study has explored methods like multi-template matching (MTM) and deformable image registration (DIR), showcasing more competitive tracking performance than PCNN[32]. Additionally, BOURQUE A E and his team used the particle filter algorithm to achieve millimeter-level tracking accuracy for lung tumors on 1.5T MRI images[29, 30]. However, they reported that out-of-plane motion poses limitations to their proposed method, a challenge also discussed by Seregni M et al[31]. In contrast, the robustness of our proposed method to this issue has been verified. The incorporation of deep learning models into tracking methods has been a recent trend, with studies by TERPSTRA M L et al. and HC Shao et al. demonstrating the potential of deep convolutional neural networks (DCNN) and improved U-net models for motion estimation[35, 36]. However, these methods necessitate large-scale datasets for pre-training, presenting challenges such as extended waiting times and generalization concerns.

The results of the aforementioned studies partially reveal the main challenges faced by MRI-based marker-less motion management and their limitations. Despite the absence of publicly available datasets for direct performance comparison, our method presents distinct advantages. This is mainly due to the characteristics of the OTLD framework, as manifested in the online updating of the detector and object model, enabling it to handle disappearances and deformations caused by out-of-plane motion. Meanwhile, the median-flow tracker ensures a consistent and precise trajectory prediction. However, algorithm optimization is still essential. The improved detector and tracker have been proven to bring significant performance enhancements, as shown in Table 1. Moreover, the proposed method's extensibility is demonstrated by its coupling with the Chan-Vese model.

On the other hand, the proposed method can accept arbitrary sequences of continuous 2D images as input and does not require pre-training, making it not specific to any imaging modality. In addition to MRI-Linacs, our method is extendable to other medical applications, such as intraoperative radiotherapy and ultrasound-guided biopsy, particularly in the field of proton therapy. The barriers ahead of the accurate proton therapy implementation were the daily imaging guidance with several imperfections: (i) not being able to see many tumors, (ii) moving tumors not being tracked directly in real-time during dose delivery, and (iii) anatomical variation and organ movement. The combination of MRI imaging and proton therapy will launch the MRI imaging guidance of proton therapy with guarantee the precise and efficacious implementation of proton dose. Our ETLD+ICV tracking method is potentially a preferable solution in the targeting accuracy of proton therapy (PT) for moving soft-tissue tumors.

It is important to acknowledge that our method has been tested solely on a 1.5T MRI dataset, and its robustness across different imaging qualities, such as the 0.35T MRI, remains to be ascertained. The variability in independently collected datasets further complicates algorithm comparisons, with equipment differences, imaging protocols, and evaluation standards contributing to this challenge. While our method has circumvented training errors due to human delineation bias, the need for publicly available datasets is accentuated. Additionally, although our algorithm reduces tracking errors, the sliding window approach can be resource-intensive, impacting clinical applicability.

Future work will incorporate other novel architectures to address the above limitations, aiming to explore potential improvements. The Region Proposal Network (RPN) is a powerful ROI generation method that can significantly enhance the localization accuracy and efficiency of

algorithms, which has been widely applied in object detection tasks[50]. Given sufficient data, RPN presents a valuable option for future research aimed at improvements. Performance validation in lower-quality data is also a subsequent goal. The quantitative evaluation of the proposed method's impact on clinical treatment outcomes remains necessary. We expect to address these questions in future studies. Meanwhile, the proposed method has already demonstrated high tracking performance in scenarios with low spatial resolution and low SNR. Considering that other imaging scenarios also exhibit such video stream characteristics, such as infrared scenes. So, we aim to apply the proposed method to similar scenarios in future research to expand its applicability.

## 5. Conclusion

In this study, an automatic real-time motion tracking method based on the ETLD+ICV method for MRIgRT has been successfully developed and validated. Results show that the enhanced TLD coupled with automatic segmentation, significantly outperforms the existing methods. The high precision and recall rates of the proposed method, without the need for pre-training, offer a promising advancement for MRIgRT applications, making it a valuable tool for improving the effectiveness of radiotherapy treatments. Our findings have implications for the broader field of radiotherapy, suggesting that the adoption of advanced tracking systems can lead to better patient outcomes. Future research could explore potential further improvements to the tracking algorithm and the possibility of applying the method in other imaging scenarios.

## References:

1. Xia, C., et al., *Cancer statistics in China and United States, 2022: profiles, trends, and determinants*. Chin Med J (Engl), 2022. **135**(5): p. 584-590.
2. Jiayun, C., et al., *A Novel High-resolution Fast Magnetic Resonance Imaging Method Incorporating BEV/BPV Fusion Information*. Nuclear Physics Review, 2024. **41**(1): p. 1-6.
3. Bertholet, J., et al., *Real-time intrafraction motion monitoring in external beam radiotherapy*. Phys Med Biol, 2019. **64**(15): p. 15TR01.
4. Liu, X., et al., *Deep learning-based target tracking with X-ray images for radiotherapy: a narrative review*. Quant Imaging Med Surg, 2024. **14**(3): p. 2671-2692.
5. Fast, M.F., et al., *Intrafraction Motion Management With MR-Guided Radiation Therapy*. Semin Radiat Oncol, 2024. **34**(1): p. 92-106.
6. Wu, V.W.C., A.P.L. Ng, and E.K.W. Cheung, *Intrafractional motion management in external beam radiotherapy*. J Xray Sci Technol, 2019. **27**(6): p. 1071-1086.
7. Poulsen, P.R., et al., *Respiratory gating based on internal electromagnetic motion monitoring during stereotactic liver radiation therapy: First results*. Acta Oncol, 2015. **54**(9): p. 1445-52.
8. Nankali, S., et al., *Geometric and dosimetric comparison of four intrafraction motion adaptation strategies for stereotactic liver radiotherapy*. Phys Med Biol, 2018. **63**(14): p. 145010.
9. Gierga, D.P., et al., *Quantification of respiration-induced abdominal tumor motion and its impact on IMRT dose distributions*. Int J Radiat Oncol Biol Phys, 2004. **58**(5): p. 1584-95.
10. Witt, J.S., S.A. Rosenberg, and M.F. Bassetti, *MRI-guided adaptive radiotherapy for liver tumours: visualising the future*. Lancet Oncol, 2020. **21**(2): p. e74-e82.
11. Yang, W.C., F.M. Hsu, and P.C. Yang, *Precision radiotherapy for non-small cell lung cancer*. J Biomed Sci, 2020. **27**(1): p. 82.
12. Gregoire, V., et al., *Image guidance in radiation therapy for better cure of cancer*. Mol Oncol, 2020. **14**(7): p. 1470-1491.
13. Dhont, J., et al., *Image-guided Radiotherapy to Manage Respiratory Motion: Lung and Liver*. Clin Oncol (R Coll Radiol), 2020. **32**(12): p. 792-804.
14. Edmunds, D., G. Sharp, and B. Winey, *Automatic diaphragm segmentation for real-time lung tumor tracking on cone-beam CT projections: a convolutional neural network approach*. Biomed Phys Eng Express, 2019. **5**(3).
15. Wei, J. and M. Chao, *A constrained linear regression optimization algorithm for diaphragm motion tracking with cone beam CT projections*. Phys Med, 2018. **46**: p. 7-15.
16. Cerviño, L.I., et al., *The diaphragm as an anatomic surrogate for lung tumor motion*. Physics in Medicine & Biology, 2009. **54**(11): p. 3529.
17. Mylonas, A., et al., *A deep learning framework for automatic detection of arbitrarily shaped fiducial markers in intrafraction fluoroscopic images*. Med Phys, 2019. **46**(5): p. 2286-2297.
18. Liang, Z., et al., *Artificial intelligence-based framework in evaluating intrafraction motion for liver cancer robotic stereotactic body radiation therapy with fiducial tracking*. Med Phys, 2020. **47**(11): p. 5482-5489.
19. Bhagat, N., et al., *Complications associated with the percutaneous insertion of fiducial markers in the thorax*. Cardiovasc Intervent Radiol, 2010. **33**(6): p. 1186-91.

20. Keall, P.J., et al., *Integrated MRI-guided radiotherapy - opportunities and challenges*. Nat Rev Clin Oncol, 2022. **19**(7): p. 458-470.
21. van Dams, R., et al., *Ablative radiotherapy for liver tumors using stereotactic MRI-guidance: A prospective phase I trial*. Radiother Oncol, 2022. **170**: p. 14-20.
22. Finazzi, T., et al., *Clinical Outcomes of Stereotactic MR-Guided Adaptive Radiation Therapy for High-Risk Lung Tumors*. Int J Radiat Oncol Biol Phys, 2020. **107**(2): p. 270-278.
23. Gao, Y., et al., *Accelerated 3D bSSFP imaging for treatment planning on an MRI-guided radiotherapy system*. Med Phys, 2018. **45**(6): p. 2595-2602.
24. Bruijnen, T., et al., *Multiresolution radial MRI to reduce IDLE time in pre-beam imaging on an MR-Linac (MR-RIDDLE)*. Phys Med Biol, 2019. **64**(5): p. 055011.
25. Zhou, S.K., et al., *A review of deep learning in medical imaging: Imaging traits, technology trends, case studies with progress highlights, and future promises*. Proc IEEE Inst Electr Electron Eng, 2021. **109**(5): p. 820-838.
26. Havsteen, I., et al., *Are Movement Artifacts in Magnetic Resonance Imaging a Real Problem? - A Narrative Review*. Front Neurol, 2017. **8**: p. 232.
27. Yun, J., et al., *Neural-network based autocontouring algorithm for intrafractional lung-tumor tracking using Linac-MR*. Med Phys, 2015. **42**(5): p. 2296-310.
28. Yun, J., et al., *Improved lung tumor autocontouring algorithm for intrafractional tumor tracking using 0.5 T linac-MR*. Biomedical Physics & Engineering Express, 2016. **2**(6): p. 067004 %U <https://dx.doi.org/10.1088/2057-1976/2/6/067004>.
29. Bourque, A.E., et al., *A particle filter motion prediction algorithm based on an autoregressive model for real-time MRI-guided radiotherapy of lung cancer*. Biomedical Physics & Engineering Express, 2017. **3**(3): p. 035001 %U <https://iopscience.iop.org/article/10.1088/2057-1976/aa6b5b>.
30. Bourque, A.E., et al., *Particle Filter-Based Target Tracking Algorithm for Magnetic Resonance-Guided Respiratory Compensation: Robustness and Accuracy Assessment*. Int J Radiat Oncol Biol Phys, 2018. **100**(2): p. 325-334.
31. Seregni, M., et al., *A Hybrid Image Registration and Matching Framework for Real-Time Motion Tracking in MRI-Guided Radiotherapy*. IEEE Trans Biomed Eng, 2018. **65**(1): p. 131-139.
32. Fast, M.F., et al., *Tumour auto-contouring on 2d cine MRI for locally advanced lung cancer: A comparative study*. Radiother Oncol, 2017. **125**(3): p. 485-491.
33. Friedrich, F., et al., *Stability of conventional and machine learning-based tumor auto-segmentation techniques using undersampled dynamic radial bSSFP acquisitions on a 0.35 T hybrid MR-linac system*. Med Phys, 2021. **48**(2): p. 587-596.
34. Dhont, J., et al., *Multi-object tracking in MRI-guided radiotherapy using the tracking-learning-detection framework*. Radiother Oncol, 2019. **138**: p. 25-29.
35. Terpstra, M.L., et al., *Real-time 3D motion estimation from undersampled MRI using multi-resolution neural networks*. Med Phys, 2021. **48**(11): p. 6597-6613.
36. Shao, H.-C., et al., *Real-time MRI motion estimation through an unsupervised k-space-driven deformable registration network (KS-RegNet)*. Physics in Medicine & Biology, 2022. **67**(13): p. 135012.
37. Kalal, Z., K. Mikolajczyk, and J. Matas, *Tracking-Learning-Detection*. IEEE Trans Pattern Anal Mach Intell, 2012. **34**(7): p. 1409-22.
38. Dong, E., et al., *Moving vehicle tracking based on improved tracking-learning-detection*

*algorithm*. IET Computer Vision, 2019. **13**(8): p. 730-741.

39. Shi, J., X. Wang, and H. Xiao, *Real-Time Pedestrian Tracking and Counting with TLD*. Journal of Advanced Transportation, 2018. **2018**: p. 1-7.

40. Mittal, A., A.K. Moorthy, and A.C. Bovik, *No-reference image quality assessment in the spatial domain*. IEEE Trans Image Process, 2012. **21**(12): p. 4695-708.

41. Chan, T.F. and L.A. Vese, *Active contours without edges*. IEEE Trans Image Process, 2001. **10**(2): p. 266-77.

42. Lewis, B., et al., *Evaluating motion of pancreatic tumors and anatomical surrogates using cine MRI in 0.35T MRgRT under free breathing conditions*. J Appl Clin Med Phys, 2023. **24**(6): p. e13930.

43. Jupitz, S.A., et al., *Investigation of tumor and vessel motion correlation in the liver*. J Appl Clin Med Phys, 2020. **21**(8): p. 183-190.

44. Rosenberg, S.A., et al., *A Multi-Institutional Experience of MR-Guided Liver Stereotactic Body Radiation Therapy*. Adv Radiat Oncol, 2019. **4**(1): p. 142-149.

45. Grama, D., et al., *Deep learning-based markerless lung tumor tracking in stereotactic radiotherapy using Siamese networks*. Med Phys, 2023. **50**(11): p. 6881-6893.

46. Bilic, P., et al., *The Liver Tumor Segmentation Benchmark (LiTS)*. Med Image Anal, 2023. **84**: p. 102680.

47. Wei, R., et al., *Real-time 3D MRI reconstruction from cine-MRI using unsupervised network in MRI-guided radiotherapy for liver cancer*. Med Phys, 2023. **50**(6): p. 3584-3596.

48. Wu, Y., J. Lim, and M.H. Yang. *Online Object Tracking: A Benchmark*. in *2013 IEEE Conference on Computer Vision and Pattern Recognition*. 2013.

49. Keall, P.J., et al., *AAPM Task Group 264: The safe clinical implementation of MLC tracking in radiotherapy*. Med Phys, 2021. **48**(5): p. e44-e64.

50. Ren, S., et al., *Faster R-CNN: Towards Real-Time Object Detection with Region Proposal Networks*. IEEE Trans Pattern Anal Mach Intell, 2017. **39**(6): p. 1137-1149.

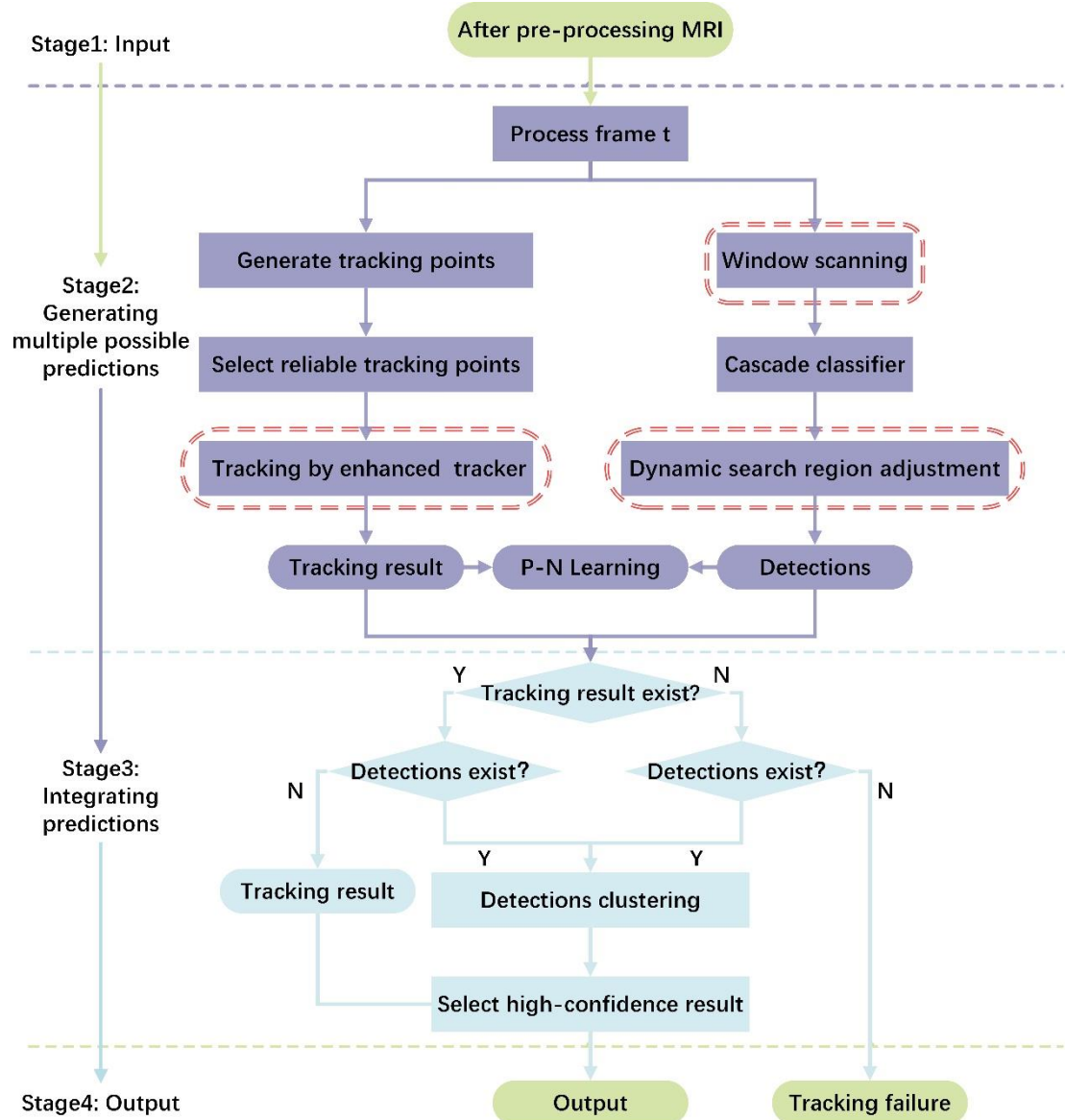


**Figure 1. The main workflow of the ETLD method. The red rounded rectangles denote the main improvements based on the OTLD.**

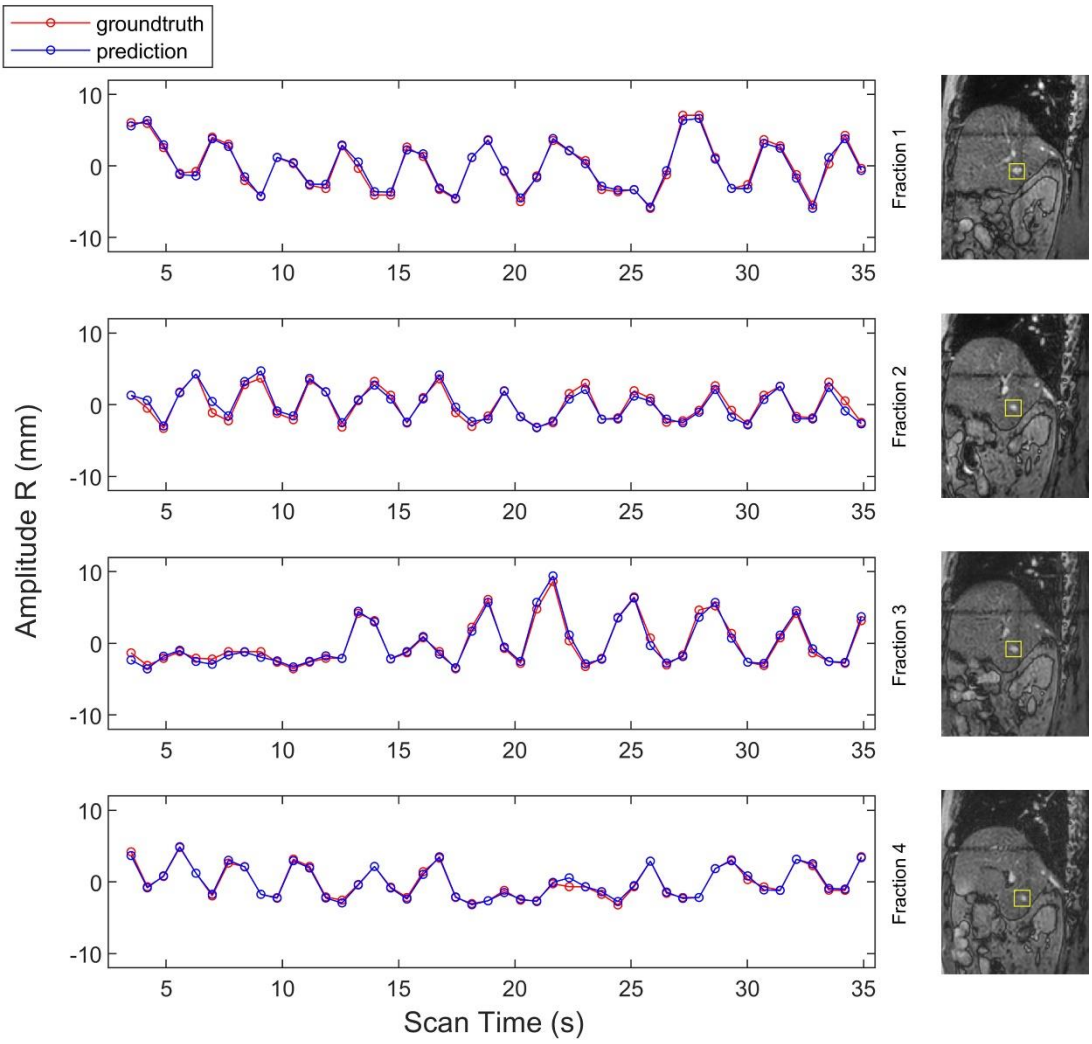


**Figure 2. The tracking results of the ETLD on patient 1's data within the RAM group at a 140-degree angle. The graph juxtaposes the actual tumor displacement (red line) with the predicted tracking (blue line), demonstrating the close correlation between the two. Accompanying images showcase the precision of tracking in representative frames, with minimal divergence between the ground truth and predictions, indicative of the algorithm's high fidelity in motion estimation.**

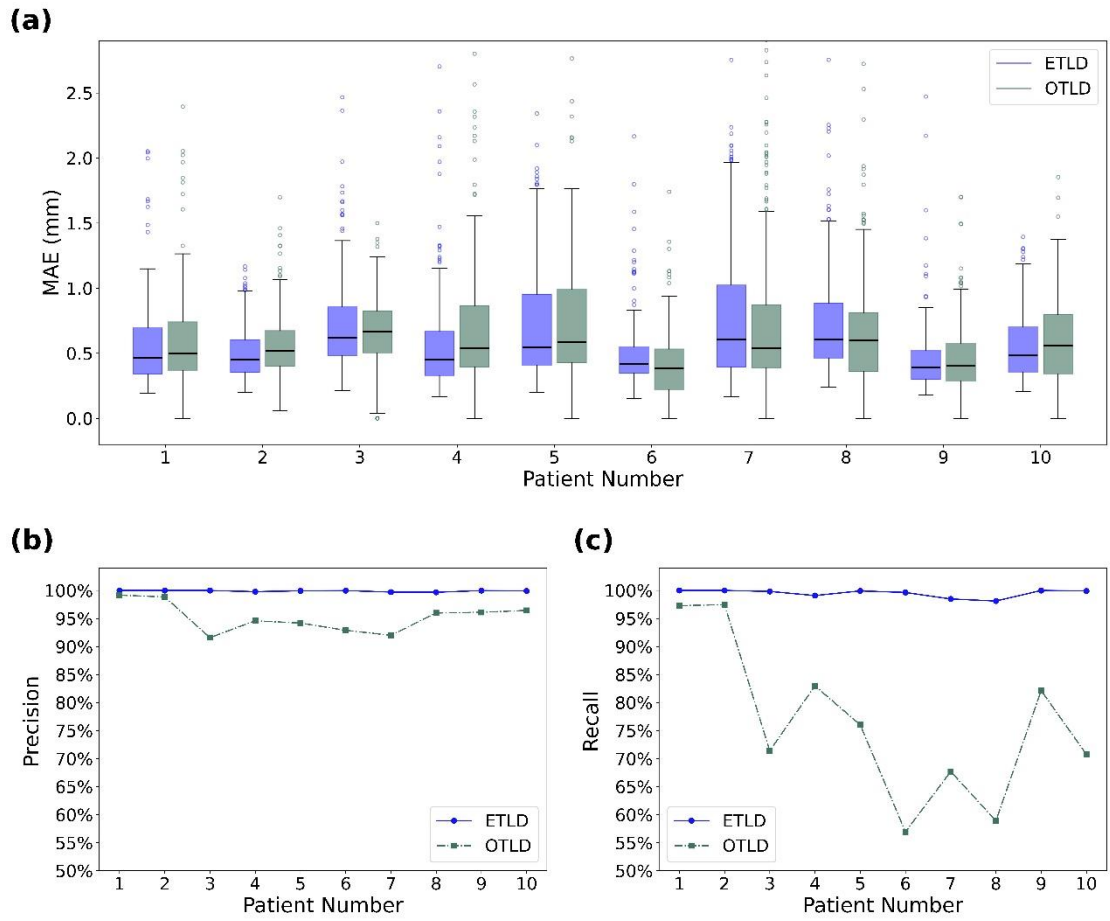


**Figure 3. Comparative tracking performance evaluation of the ETLD and the OTLD methods across multiple patients (n=10). (a) The box plot of the MAE in tracking accuracy. (b) The line plot of the precision in tracking. (c) The line plot of the recall in tracking.**

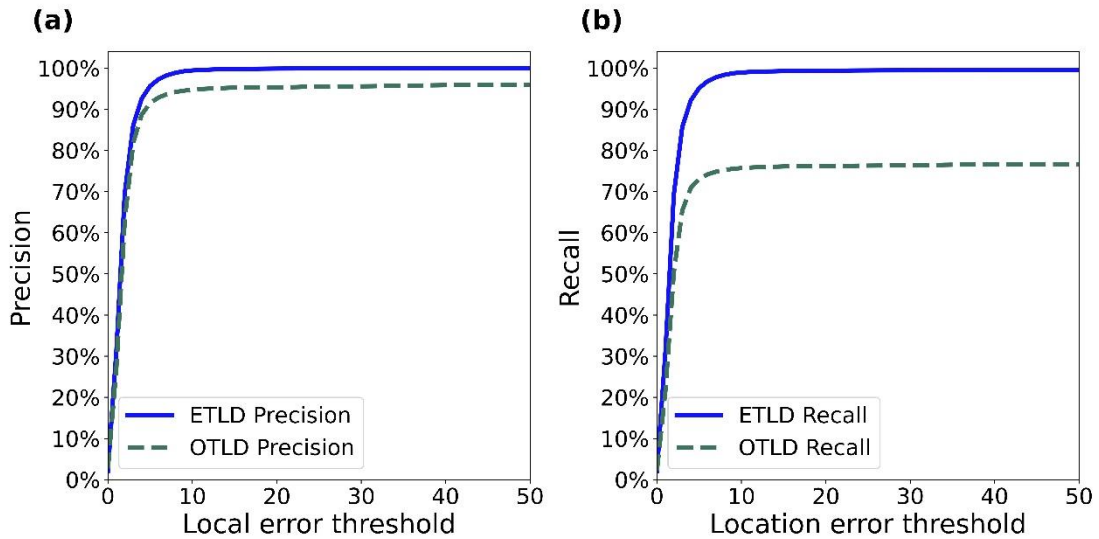


**Figure 4. The precision and recall plot of the ETLD and OTLD methods. (a) The precision plot. (b) The recall plot.**

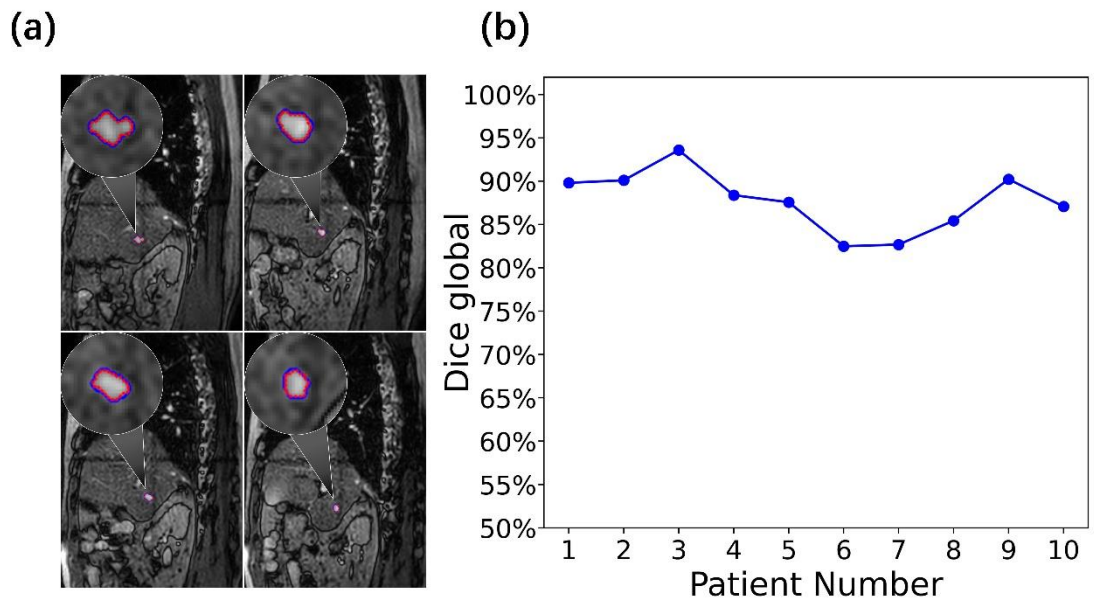


**Figure 5. Segmentation accuracy assessment of the ETLD+ICV method. (a) Direct comparison of segmentation masks for a sample patient, with ground truth in red and predictions in blue. (b) Compilation of dice global values, evidencing the segmentation accuracy across all test patients (n=10).**

**Table 1. Comparative analysis of tracking performance metrics between the ETLD and OTLD algorithms across multiple patients (n=10). The table displays MAE in millimeters, CC, precision, and recall rates for each patient and the aggregate data.**

| Patient | MAE (mm)    |             | CC    |       | Precision |       | Recall |       |
|---------|-------------|-------------|-------|-------|-----------|-------|--------|-------|
|         | ETLD        | OTLD        | ETLD  | OTLD  | ETLD      | OTLD  | ETLD   | OTLD  |
| 1       | 0.602±0.495 | 0.664±0.521 | 94.3% | 93.6% | 100.0%    | 99.2% | 100.0% | 97.3% |
| 2       | 0.493±0.188 | 0.565±0.238 | 98.5% | 98.0% | 100.0%    | 98.8% | 100.0% | 97.5% |
| 3       | 0.747±0.478 | 0.760±0.718 | 97.3% | 97.0% | 100.0%    | 91.6% | 99.8%  | 71.4% |
| 4       | 0.634±0.577 | 0.773±0.586 | 95.2% | 91.0% | 99.8%     | 94.6% | 99.1%  | 83.0% |
| 5       | 0.736±0.481 | 1.072±1.229 | 96.0% | 93.1% | 99.9%     | 94.2% | 99.9%  | 76.0% |
| 6       | 0.529±0.436 | 0.498±0.272 | 95.7% | 96.2% | 100.0%    | 92.9% | 99.6%  | 56.9% |
| 7       | 0.786±0.514 | 0.789±0.639 | 96.7% | 93.4% | 99.7%     | 92.0% | 98.5%  | 67.7% |
| 8       | 0.734±0.396 | 0.766±0.476 | 95.2% | 94.1% | 99.7%     | 96.0% | 98.1%  | 58.9% |
| 9       | 0.452±0.256 | 0.532±0.478 | 94.6% | 92.8% | 100.0%    | 96.1% | 100.0% | 82.1% |
| 10      | 0.565±0.272 | 0.671±0.565 | 96.8% | 93.9% | 99.9%     | 96.4% | 99.9%  | 70.8% |
| All     | 0.633±0.436 | 0.700±0.611 | 96.2% | 94.5% | 99.9%     | 95.3% | 99.4%  | 76.2% |